Distributed and Asynchronous Active Fault Management for Networked Microgrids

Wenfeng Wan, *Student Member, IEEE,* Mikhail A. Bragin, *Member, IEEE,* Bing Yan, *Member, IEEE,* Yanyuan Qin, *Student Member, IEEE,* Jason Philhower, *Senior Member, IEEE,* Peng Zhang, *Senior Member, IEEE,* and Peter B. Luh, *Life Fellow, IEEE*

***Abstract*—A distributed and asynchronous active fault management (DA-AFM) method is developed to manage networked microgrids' (NMs) performance under balanced or unbalanced grid faults. The DA-AFM aims to (1) enable NMs' fast fault ride-through capabilities, (2) limit the total fault contributions by coordinating heterogeneous microgrids in the NM system, and (3) deploy software-defined networks (SDN) to ensure highly resilient AFM. The problem is formulated in an optimization form that can incorporate various fault management objectives and constraints in a programmable and flexible fashion. The scalability and resiliency of the DA-AFM system are guaranteed by adopting an SDN-enabled distributed and asynchronous surrogate Lagrangian relaxation (DA-SLR) algorithm, which avoids single point of failure, preserves privacy, and eliminates the idle waiting of other subproblems. Case studies are performed on a six-microgrid NM system to validate the effectiveness and efficacy of DA-AFM. Testing results show that DA-AFM has excellent convergence performance, supports plug-and-play, is resilient to communication delay and failures, meets real-time requirements and is scalable.**

***Index Terms*—Networked microgrids, active fault management, distributed optimization, Software-Defined Networking**

I. Introduction

ACTIVE Fault Management (AFM) has been proposed in recent years [1] to promote interconnection among networked microgrids (NMs). AFM aims to 'systematically support grid resiliency under grid disturbances rather than negatively impacting the disturbed grid' [2]. The purpose of developing AFM for NMs is to address major hurdles in integrating NMs into a distribution network. First, a minor fault in the main grid could cause the microgrids to disconnect because the inverter-dominant microgrids are highly sensitive to grid anomalies. Unexpected disconnections can increase the risk of major blackouts during large grid disturbances. For this reason, the latest IEEE 1547 Standard [3] requires that microgrids be able to ride through grid faults for extended time intervals. This requirement, however, has led to the second challenge: when riding through faults, NMs can inject large fault currents that exceed the fault current limits for grid equipment, causing catastrophic damage and potential instabilities in the main grid [2] (see Fig. 1). To resolve the aforementioned challenges, an AFM system should achieve the following major goals: 1) fault ride-through that accommodates evolving grid conditions; 2) distributed and asynchronous coordination to control fault current contributions, preserve privacy, provide redundancy, and increase computation efficiency; and 3) ultra-fast and resilient NM communication that empowers real-time AFM responses to grid faults [4].

A major difficulty for fault ride-through is the complex ride-through objectives and constraints in microgrids. Current limiters used in Ref. [5], [6] and converter controls used in Ref. [7], [8] can effectively limit fault currents from individual microgrids, but they lack the ability to mitigate power ripples and cannot maintain power flow balance before and after faults. Although some existing methods use reference-frame-based control to manage power ripples in grid-tied converters [9], [10]in ways that may help improve power quality, they are unable to effectively support the main grid and manage NMs' fault current contributions [11], [12].

During NMs' ride-through, uncoordinated microgrids' fault contributions may exceed the safety limits for major equipment, thus hampering the adoption of NMs. The fault contributions of multiple microgrids must be coordinated in real time to avoid monotonically increasing fault currents due to new microgrid interconnections. Preliminary research for a centralized AFM scheme has shown the effectiveness of AFM in limiting fault contributions from individual microgrids [11] and networked microgrids [12]. In reality, however, microgrid owners/stakeholders tend to avoid disclosing their private data to neighboring microgrids or a third party coordinator such as a utility control center. Privacy preservation and security concerns have made distributed methods a desirable choice for AFM solutions. Asynchronous schemes can eliminate the idle waiting of subproblems in distributed computing. Despite the advantages of avoiding single point of failures and supporting plug-and-play [13], [14], distributed methods face significant challenges of scalability and efficiency in solving large NM problems such as AFM. Adding to those challenges is the fact that nearly all published distributed optimization based solutions for microgrids are implemented on one central processing unit (CPU) in a pseudo distributed way [15]–[17]. As a result, so far, no literature has exploited truly distributed solutions for AFM in NMs.

This work was supported in part by the National Science Foundation under Grants ECCS-1611095, CNS-1647209 and ECCS-1831811, and in part by the Office of the Provost, University of Connecticut.

W. Wan and P. Zhang are with the Department of Electrical and Computer Engineering, Stony Brook University, Stony Brook, NY 11794, USA. (e-mail: p.zhang@stonybrook.edu).

M. A. Bragin, J. Philhower, and P. B. Luh are with the Department of Electrical and Computer Engineering, University of Connecticut, Storrs, CT 06269, USA.

B.Yan is with the Department of Electrical and Microelectronic Engineering, Rochester Institute of Technology, Rochester, NY 14623, USA.

Y. Qin is with the Department of Computer Science and Engineering, University of Connecticut, Storrs, CT 06269, USA.

This article has been accepted for publication in a future issue of this journal, but has not been fully edited. Content may change prior to final publication. Citation information: DOI 10.1109/TPWRS.2020.2976044, IEEE Transactions on Power Systems

The third challenge is the need for an NM communication network that will ensure the fast and resilient data transmission required for AFM. Mainly because of the plug-and-play of microgrids or microgrid components, existing hardware-dependent communication networking techniques [18] [19] cannot cost-effectively update network configurations and policies to adapt to ever-changing NM conditions and topologies [20]. A resilient AFM requires an automatic, ultra-fast, and reconfigurable network that can respond to communication delays, link losses, and various attacks [18].

To address the above challenges, this paper presents a distributed and asynchronous AFM solution (DA-AFM, illustrated in Fig. 1). The salient features of DA-AFM include:

- DA-AFM is formulated as a distributed optimization problem that supports customized requirements and the plug-and-play of microgrids or microgrid components. Any AFM objectives such as currents or powers can be added into or removed from the formulation easily.
- A distributed and asynchronous surrogate Lagrangian relaxation (DA-SLR) method is devised to coordinate various microgrids during faults. AFM for each individual microgrid is computed on a separate core. This computation scheme leads to a genuine distributed and asynchronous algorithm.
- A software-defined networking (SDN) architecture [4] for enabling low-latency distributed computing is integrated to empower DA-AFM, making it hardware-independent, fast and programmable, and resilient to communication delay and link loss by the ultra-fast activation of backup channels.

The remainder of this paper is organized as follows. Section II gives the formulation of centralized AFM, based on which the formulation and multi-core implementation of DA-AFM are given in Section III. Section IV presents various case studies related to different types of faults and topologies, plug-and-play, immunity to communication delay, real-time performance and scalability. Conclusions and future work are discussed in Section V.

II. Problem Formulation

AFM is formulated as a nonlinear multi-objective optimization problem, with its objectives and constraints modifiable on a case-by-case basis, allowing it to adapt to the evolving conditions and operational requirements that are likely to occur during the life cycle of an NM system [11], [12], [21].

In the formulation, voltage vectors ($\mathbf{U}$) and current vectors ($\mathbf{I}$) are written into real and imaginary components in rectangular coordinates. In our study, AFM minimizes the weighted sum of two objectives: F_1 and F_2. F_1 is the NMs' contributions in increasing the main grid's fault currents. F_2 is the double-line-frequency ripples in output instantaneous power that microgrids deliver to the main grid. Fault current contributions mean how large fault currents' amplitudes, $\|\mathbf{I}\|$, have been increased because of the integration of NMs. Because total fault currents are vector additions of the main grid's fault currents and NMs' fault currents, total fault currents and main grid's fault currents can have the same amplitude even when NMs' fault currents are not zero. This situation means the integration of NMs has little effect on the main grid. This

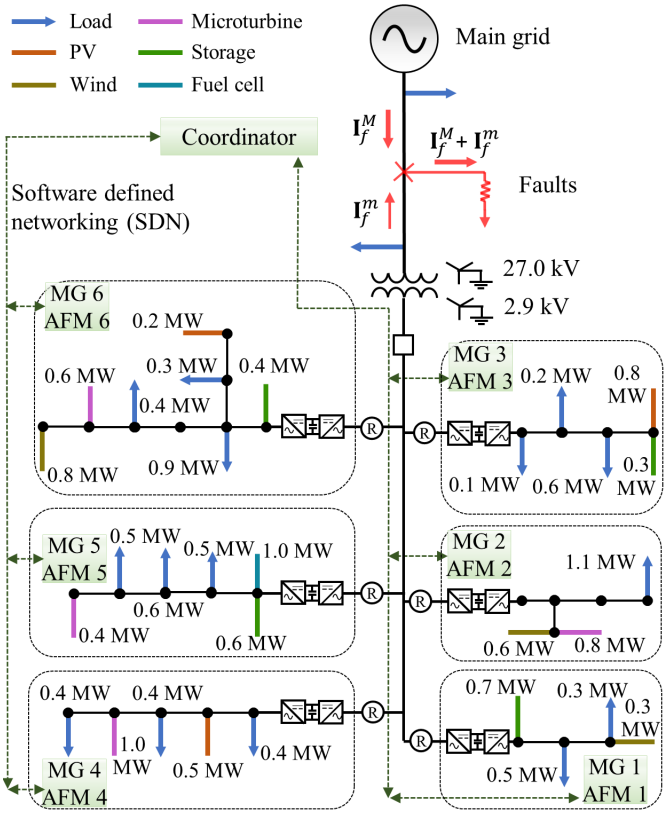

Fig. 1. Schematic of distributed and asynchronous active fault management (DA-AFM) for networked microgrids (NMs).

can be achieved by adjusting NMs currents' amplitudes and angles.

A centralized formulation of AFM [2] is expressed as follows:

$$\min \qquad \alpha F_1 + (1-\alpha)F_2, \quad \alpha \in [0,1] \tag{1}$$

s.t.

$$\textstyle\sum_j [\mathrm{Re}(\mathbf{U}_{i,j})\mathrm{Re}(\mathbf{I}_{i,j}) + \mathrm{Im}(\mathbf{U}_{i,j})\mathrm{Im}(\mathbf{I}_{i,j})] = P_i \tag{2}$$

$$\textstyle\sum_j \mathbf{I}_{i,j} = \mathbf{0} \tag{3}$$

$$[\mathrm{Re}(\mathbf{I}_{i,j})]^2 + [\mathrm{Im}(\mathbf{I}_{i,j})]^2 \le (I_i^S)^2 \tag{4}$$

$$[\mathrm{Re}(\sum_{i=1}^{N} \mathbf{S}_i \mathbf{I}_{i,j})]^2 + [\mathrm{Im}(\sum_{i=1}^{N} \mathbf{S}_i \mathbf{I}_{i,j})]^2 \le (I^{S,M})^2 \tag{5}$$

where

$$\begin{cases} F_1 \equiv \frac{1}{D}\sum_f \left| \frac{[\mathrm{Re}(\mathbf{I}_f^M + \mathbf{I}_f^m)]^2 + [\mathrm{Im}(\mathbf{I}_f^M + \mathbf{I}_f^m)]^2}{[\mathrm{Re}(\mathbf{I}_f^M)]^2 + [\mathrm{Im}(\mathbf{I}_f^M)]^2} - 1 \right| \\ \mathbf{I}_f^m \equiv \sum_{i=1}^{N} (\mathbf{S}_i \mathbf{I}_{i,f}) \\ F_2 \equiv \frac{1}{N}\sum_{i=1}^{N} \frac{R_i}{(P_i)^2} \\ R_i \equiv \{\sum_j [\mathrm{Re}(\mathbf{U}_{i,j})\mathrm{Re}(\mathbf{I}_{i,j}) - \mathrm{Im}(\mathbf{U}_{i,j})\mathrm{Im}(\mathbf{I}_{i,j})]\}^2 \\ \qquad + \{\sum_j [\mathrm{Im}(\mathbf{U}_{i,j})\mathrm{Re}(\mathbf{I}_{i,j}) + \mathrm{Re}(\mathbf{U}_{i,j})\mathrm{Im}(\mathbf{I}_{i,j})]\}^2 \\ (i = 1, ..., N; j = a, b, c; f \in \mathcal{P}(\{a, b, c\}). \end{cases} \tag{6}$$

This article has been accepted for publication in a future issue of this journal, but has not been fully edited. Content may change prior to final publication. Citation information: DOI 10.1109/TPWRS.2020.2976044, IEEE Transactions on Power Systems

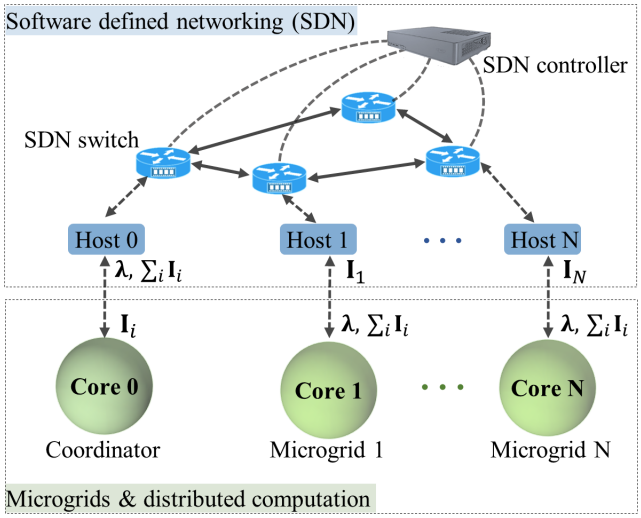

Fig. 2. Schematic of SDN-enabled DA-AFM, which is implemented within one CPU of multiple cores. $\mathbf{I}_i$ is microgrid i's currents.

In the formulation provided above, N is the total number of microgrids in the NMs. Superscripts M and m denote variables in the main grid and NMs, respectively. The superscript S indicates current safety ratings. Subscript i represents microgrid i. Subscripts j and f denote all three phases (a, b, c) and faulted phases, respectively. If only phase a encounters ground faults, then f is a. If both phases a and b encounter ground faults, then f are a and b. Symbol $\mathcal{P}$ indicates all subsets.

The weight factor α represents the trade-off between F_1 and F_2 . The complex number $\mathbf{S}_i$ represents the change induced by the transformer on microgrid i's currents when they flow to fault locations. The active power microgrid i delivers to the main grid is denoted as P_i. Here, I_i^S is the current rating for the interface between microgrid i and the main grid, and $I^{S,M}$ is the current rating of the tie line between the main grid and the NMs. Microgrid i's six decision variables are $\text{Re}(\mathbf{I}_{i,j})$ and $\text{Im}(\mathbf{I}_{i,j})(j = a, b, c)$, and the total number of decision variables in (1)-(6) is $6N$.

In F_1, $\sqrt{[\text{Re}(\mathbf{I}_f^M)]^2 + [\text{Im}(\mathbf{I}_f^M)]^2}$, $\sqrt{[\text{Re}(\mathbf{I}_f^m)]^2 + [\text{Im}(\mathbf{I}_f^m)]^2}$ are fault currents to the ground from the main grid and NMs, respectively. $\sqrt{[\text{Re}(\mathbf{I}_f^M + \mathbf{I}_f^m)]^2 + [\text{Im}(\mathbf{I}_f^M + \mathbf{I}_f^m)]^2}$ are the total fault currents, the sum of the main grid and NMs' fault currents. In F_2, $\sqrt{R_i}$ is the amplitude of microgrid i's power ripples. In AFM's weighted sum (1), the square roots are removed and the scaling factor D is introduced to rescale, as an effort to improve computation speed and accuracy.

For AFM's four constraints, (2) is the power balance before and after faults to avoid a large increase in capacitors' voltages inside the microgrids and to avoid further disturbances induced by large changes in the power flow. Constraint (3) is to null zero-sequence currents to make AFM applicable to various grounding systems, converters, and transformers. Constraints (4) and (5) are current ratings for the microgrid i and the tie line between the main grid and the NMs, respectively.

Algorithm 1: Distributed and asynchronous active fault management (DA-AFM) for networked microgrids

Result: N microgrids' output currents $\mathbf{I}_i (i = 1, ..., N)$
initialization: N microgrids' currents $\mathbf{I}_i^0 (i = 1, ..., N)$, Lagrange multipliers $\boldsymbol{\lambda}^0$, updating step size ϵ^0, termination criterion σ
iteration $k \leftarrow 1$
while $\|\boldsymbol{\lambda}^k - \boldsymbol{\lambda}^{k-1}\| > \sigma$ **do**
  N microgrids optimize distributedly with SQP based on (7)-(13);
  Microgrid i' finishes its optimization, outputs its currents $\mathbf{I}_{i'}^k$;
  The coordinator updates $\boldsymbol{\lambda}^k$ asynchronously with $\mathbf{I}_{i'}^k$ and $\mathbf{I}_i^{k-1}$ $(i = 1, ..., i' - 1, i' + 1, ..., N)$ based on (14);
  iteration $k \leftarrow k + 1$
end

III. Method and Implementation of DA-AFM

This section first introduces the application of DA-SLR in AFM, rendering AFM distributed and asynchronous. DA-SLR is mathematically proved to converge even when the updating sequence of subproblems is unknown a priori. Then DA-AFM's implementation in multiple cores and its real-time realization are explained.

A. Application of DA-SLR

Among the constraints of centralized AFM systems, constraint (5) is a system-wide coupling constraint that couples all the microgrids and is relaxed with Lagrange multipliers $\boldsymbol{\lambda}$ [22], [23]. The resulting relaxed problem is decomposed into N subproblems, with each subproblem representing the AFM of an individual microgrid. AFM for microgrid i' at iteration k is formulated in (7)-(13). Variables $\text{Re}(\mathbf{I}_{i',j})$ and $\text{Im}(\mathbf{I}_{i',j})(j = a, b, c)$ are six decision variables of microgrid i', i.e., microgrid i''s output currents to the main grid.

$$\min \quad \alpha F_{i',1} + (1 - \alpha) F_{i',2} + \boldsymbol{\lambda}^T \boldsymbol{g}, \quad \alpha \in [0, 1] \tag{7}$$

s.t.

$$\textstyle\sum_j [\text{Re}(\mathbf{U}_{i',j})\text{Re}(\mathbf{I}_{i',j}) + \text{Im}(\mathbf{U}_{i',j})\text{Im}(\mathbf{I}_{i',j})] = P_{i'} \tag{8}$$

$$\textstyle\sum_j \mathbf{I}_{i',j} = \mathbf{0} \tag{9}$$

$$(\text{Re}(\mathbf{I}_{i',j}))^2 + (\text{Im}(\mathbf{I}_{i',j}))^2 \leq (I_{i'}^S)^2 \tag{10}$$

where

$$\begin{cases} F_{i',1} \equiv \frac{1}{D} \sum_f \left| \frac{[\text{Re}(\mathbf{I}_f^M + \mathbf{I}_f^m)]^2 + [\text{Im}(\mathbf{I}_f^M + \mathbf{I}_f^m)]^2}{[\text{Re}(\mathbf{I}_f^M)]^2 + [\text{Im}(\mathbf{I}_f^M)]^2} - 1 \right| \\ \mathbf{I}_f^m \equiv \sum_{i=1, i \neq i'}^{N} (\mathbf{S}_i \mathbf{I}_{i,f}^{k-1}) + \mathbf{S}_{i'} \mathbf{I}_{i',f} \end{cases} \tag{11}$$

$$F_{i',2} \equiv \frac{R_{i'}}{(P_{i'})^2} \tag{12}$$

This article has been accepted for publication in a future issue of this journal, but has not been fully edited. Content may change prior to final publication. Citation information: DOI 10.1109/TPWRS.2020.2976044, IEEE Transactions on Power Systems

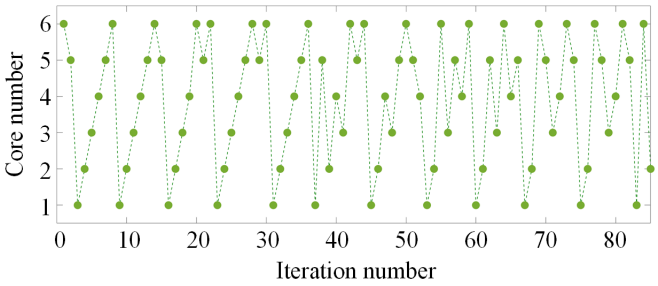

Fig. 3. Calculation sequence with six microgrids for one calculation of DA-AFM. Each core solves one microgrid's AFM.

$$g_j \equiv [\mathrm{Re}(\sum_{i=1,i\neq i'}^{N} \mathbf{S}_i \mathbf{I}_{i,j}^{k-1} + \mathbf{S}_{i'} \mathbf{I}_{i',j})]^2 + [\mathrm{Im}(\sum_{i=1,i\neq i'}^{N} \mathbf{S}_i \mathbf{I}_{i,j}^{k-1} + \mathbf{S}_{i'} \mathbf{I}_{i',j})]^2 - (I^{S,M})^2 \quad (13)$$
$$(j = a, b, c; f \in \mathcal{P}(\{a, b, c\}).$$

In the above, $\boldsymbol{\lambda} = [\lambda_a, \lambda_b, \lambda_c]$ and $\boldsymbol{g} = [g_a, g_b, g_c]$, both 3-dimensional vectors, represent Lagrange multipliers and violations levels of the relaxed constraint (5), respectively. All the other letters, superscripts and subscripts have the same meanings as in (1)-(6).

The subproblem (7) to (13) is solved with sequential quadratic programming (SQP). Subproblem solutions are coordinated by the coordinator, e.g., the distribution network operator, through updating Lagrange multipliers based on

$$\boldsymbol{\lambda}^{k+1} = max(\boldsymbol{\lambda}^k + \epsilon^k \boldsymbol{g}^k, \mathbf{0}) \quad (14)$$

where k is the iteration number; ϵ^k is the stepsize; and $\boldsymbol{g}^k$ is penalty for constraint violations, as given by (13). The coordinator updates $\boldsymbol{\lambda}$ immediately after the coordinator receives the subproblem solution of (7)-(13) from one microgrid without waiting for other microgrids to finish, making DA-AFM asynchronous.

DA-SLR's convergence has been proved mathematically [22] for separable problems where each subproblem is independent of other subproblems' solutions. In DA-AFM, subproblems' solutions are not independent because of the quadratic terms in (11) and (13) that couple currents from all microgrids. Nevertheless, when subproblems (7)-(13) are solved subject to the surrogate optimality condition, $L(\boldsymbol{\lambda}^k, \mathbf{I}^k) < L(\boldsymbol{\lambda}^k, \mathbf{I}^{k-1})$ with $L = \alpha F_1 + (1-\alpha)F_2 + \boldsymbol{\lambda}^T \boldsymbol{g}$, the resulting multiplier-updating direction also forms acute angles with directions toward the optimum. Surrogate optimality condition being satisfied together with the step sizing formula developed in [24] guarantee convergence. DA-AFM's convergence is demonstrated numerically in section IV.

B. Multi-core implementation of SDN-enabled DA-AFM

Existing distributed optimization solutions are usually pseudo distributed [15], [16]. All the subproblems are solved in one computation core, and the subproblems' computation sequence is predefined. By contrast, our implementation of DA-AFM is truly distributed and asynchronous, since each subproblem is assigned to a different core and the calculation sequence is determined by cores' computation capability.

Fig.2 shows the DA-AFM's implementation with multiple cores within one CPU. The data transfer between microgrids

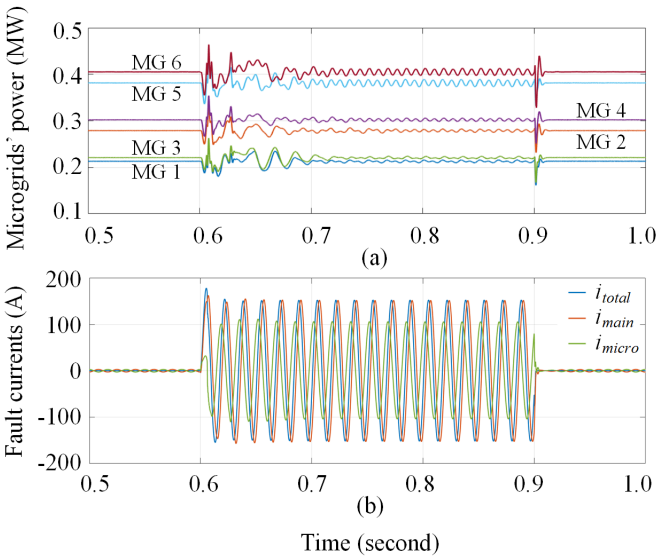

Fig. 4. DA-AFM for networked microgrids during single-phase-to-ground fault: (a) six microgrids' output power; (b) phase a currents at the fault location. i_{total} are the total fault currents to the ground. i_{main} and i_{micro} are fault currents from the main grid and NMs, respectively.

and the coordinator is managed by SDN. One breakthrough of SDN is to decouple the control plane (SDN controllers) from the data plane (SDN switches). For this architecture, controllers with a global network view can quickly implement new policies, e.g., rerouting in response to link delay and loss. This eliminates the time-consuming process of waiting for switches or routers, which have limited knowledge and authority, to figure out how to respond.

Before computation, core i' receives the newest value of $\boldsymbol{\lambda}$ and $\sum_i \mathbf{I}_i$ (Lagrange multipliers and NMs' output currents, respectively) from the coordinator. After computation, core i' sends subproblem i''s solutions $\mathbf{I}_{i'}$ (microgrid i''s output currents) to the coordinator. The coordinator, realized by another individual core, will update $\boldsymbol{\lambda}$ and $\sum_i \mathbf{I}_i$ immediately after receiving microgrid i''s updated outputs without waiting for the other microgrids/cores' results. Algorithm 1 shows the computation process of DA-AFM.

As shown in Fig. 2 and Algorithm 1, each microgrid and its computation core computes asynchronously, and the coordinator updates without waiting for other microgrids' computation. DA-AFM supports smooth and convenient plug-and-play. After the connection or disconnection of certain microgrids, no change is required for each microgrids' algorithm. The only slight change is the computation of $\sum_i \mathbf{I}_i$ at the coordinator. DA-AFM's distributed and asynchronous nature can better facilitate NMs' future development, where heterogeneous microgrids of different owners and computational capacities will be connected together to further microgrids' benefits. Fig. 3 shows a calculation sequence for DA-AFM with six microgrids.

One issue of modeling AFM as an optimization problem is real-time realization, since optimization usually takes longer than conventional feedback control. To enable real-time DA-AFM, the following strategies can be taken, all at a price of worsening of performance to an acceptable degree. The first

This article has been accepted for publication in a future issue of this journal, but has not been fully edited. Content may change prior to final publication. Citation information: DOI 10.1109/TPWRS.2020.2976044, IEEE Transactions on Power Systems

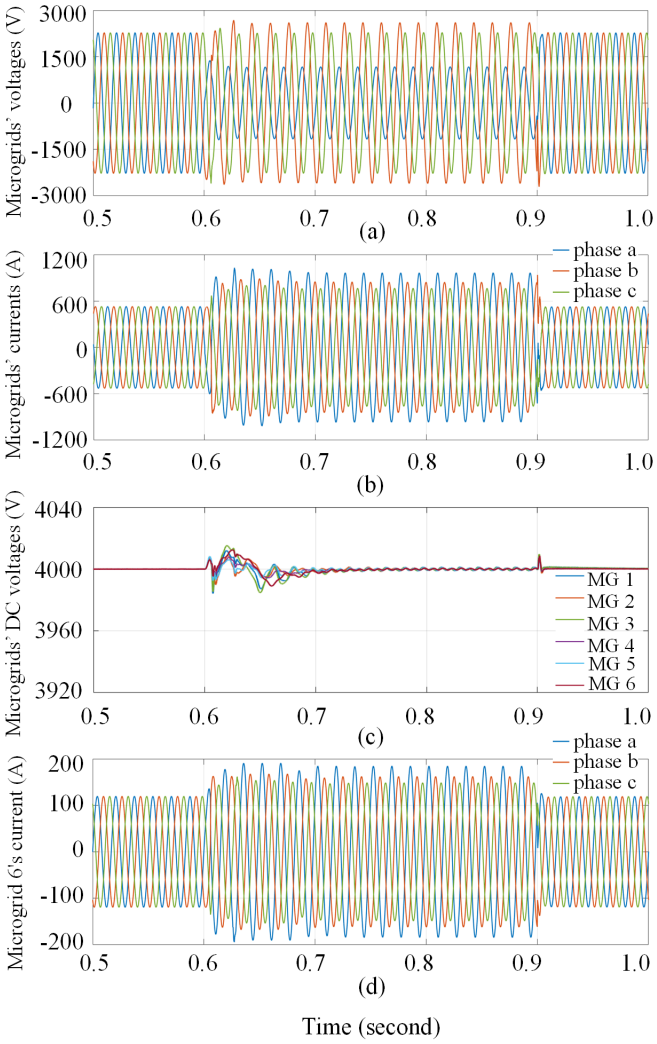

Fig. 5. DA-AFM for networked microgrids during single-phase-to-ground fault: (a) NMs' voltages at connection point; (b) NMs' currents to the main grid; (c) NMs' DC voltages; (d) microgrid 6's currents.

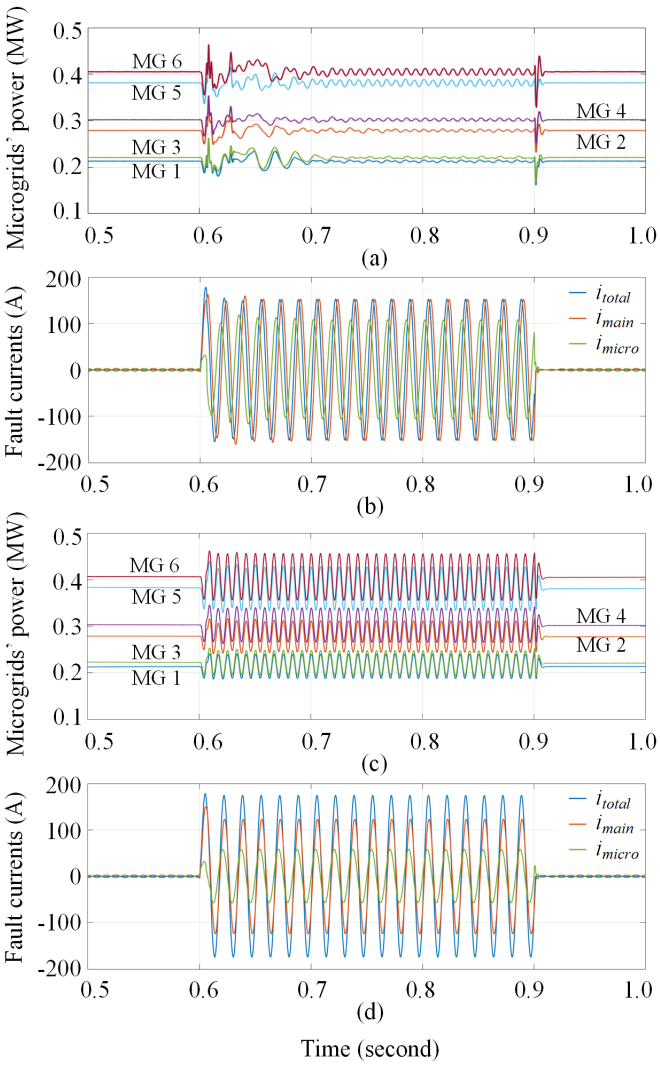

Fig. 6. Centralized AFM during single-phase-to-ground fault: (a) microgrids' output power and (b) fault currents at the fault location. The simple ride-through method during single-phase-to-ground fault: (c) microgrids' output power and (d) fault currents at the fault location.

strategy is to make optimization modules and feedback control modules asynchronous so that feedback control modules use the newest available results from the optimization modules without waiting for the optimization modules' current computation. Second, the number of optimizations' iterations can be reduced by increasing the stop criteria and by providing look-up tables for initial values.

IV. Case Study

DA-AFM is verified on a six-microgrid NM system (Fig. 1), implemented on a DELL PowerEdge R740. Single-phase and double-phase ground faults, both occurring in the main grid, have been studied. The weight factor α in (1) and (7) is set to 0.95, which can be chosen from the Pareto frontier based on requirements. DA-AFM has been compared with centralized AFM and a simple ride-through method. DA-AFM's plug-and-play and its immunity to communication delays are also demonstrated.

Every microgrid in the NMs connects to the main grid through a back-to-back converter at the same point of connection. Before faults, the active power delivered to the main grid by microgrid 1 to microgrid 6 are 213 kW, 278 kW, 221 kW, 302 kW, 381 kW and 407 kW, respectively, without any transfer of reactive power. Each microgrid's delivered power is one quarter of its capacity, and the left three quarters are consumed by their own loads inside the microgrids.

Centralized AFM, with comprehensive access to information from all of the microgrids, is simulated to demonstrate DA-AFM's accurate convergence. The formulation of centralized AFM, (1) to (6), is solved directly with SQP. Without iterative updating from individual microgrids, centralized AFM doesn't have divergence issues.

A simple ride-through method is simulated to demonstrate DA-AFM's superiority. This simple ride-through method manages power balance, the microgrids' DC voltages, and the microgrids' output currents. This method belongs to PQ control strategy [25]–[27]. However, it doesn't consider power ripples or whether NMs would increase fault currents at fault locations.

According to the following results, DA-AFM converges as

This article has been accepted for publication in a future issue of this journal, but has not been fully edited. Content may change prior to final publication. Citation information: DOI 10.1109/TPWRS.2020.2976044, IEEE Transactions on Power Systems

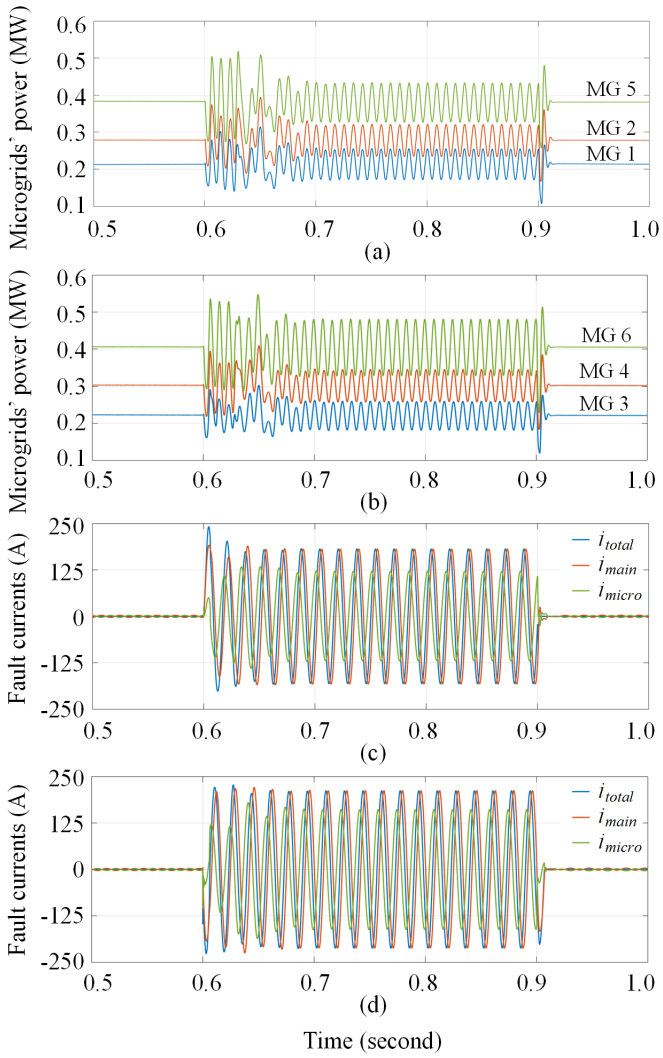

Fig. 7. DA-AFM for networked microgrids during double-phase-to-ground fault: (a) six microgrids' output power; (b) phase a fault currents at fault location; (c) phase b fault currents at fault locations. i_{total} is the total fault currents to the ground. i_{main} and i_{micro} are fault currents from the main grid and NMs, respectively.

accurately as centralized AFM and performs better than the simple ride-through method. It should be noted that DA-AFM is more compatible with the future expansion, privacy, and cybersecurity needs of NMs.

A. Single-phase-to-ground (SPG) fault

In this case study, a SPG fault happens on phase a from 0.6s to 0.9s. The remaining voltage is 0.52 pu. The results of DA-AFM are shown in Fig. 4 (NMs' power and phase a currents at the fault location) and Fig. 5 (NMs' voltages, currents, and DC voltages). As shown in Fig. 4, fault currents from the main grid and the total fault currents are controlled to be the same at 152.21 A, meaning NMs' contribution to fault currents is 0.00%. Power ripples of six microgrids are 0.79%, 1.00%, 0.47%, 0.95%, 1.80% and 1.63%, respectively, averaging 1.11%.

Fig. 6 shows the results with centralized AFM and the simple ride-through method for SPG fault. In centralized AFM (Fig. 6 (a) and (b)), the fault current contribution is 0.00% and six microgrids' power ripples are 1.23%, 1.21%, 1.16%, 1.04%, 0.83% and 2.03%, respectively, with an average value of 1.25%. In the simple ride-through method (Fig. 6 (c) and (d)), the fault current contribution is 14.68% (174.55/152.21), and six microgrids' power ripples are 12.21%, 12.41%, 12.22%, 12.42% and 12.47% and 12.32%, respectively, with an average value of 12.34%.

TABLE I
COMPARISON BETWEEN DIFFERENT FAULT MANAGEMENT METHODS FOR SINGLE-PHASE-TO-GROUND FAULT

	DA-AFM		A simple ride-through method		Centralized AFM	
	fault contribution	power ripples	fault contribution	power ripples	fault contribution	power ripples
MG 1	0.00%	0.79%	14.68%	12.21%	0.00%	1.23%
MG 2		1.00%		12.41%		1.21%
MG 3		0.47%		12.22%		1.16%
MG 4		0.95%		12.42%		1.04%
MG 5		1.80%		12.47%		0.83%
MG 6		1.63%		12.32%		2.03%
Average	0.00%	1.11%	14.68%	12.34%	0.00%	1.25%

TABLE II
COMPARISON BETWEEN DIFFERENT FAULT MANAGEMENT METHODS FOR DOUBLE-PHASE-TO-GROUND FAULT

	DA-AFM		A simple ride-through method		Centralized AFM	
	fault contributions	power ripples	fault contributions	power ripples	fault contributions	power ripples
MG 1	0.00% (ϕ a); 0.00% (ϕ b)	19.48%	26.82% (ϕ a); 16.97% (ϕ b)	27.46%	0.00% (ϕ a); 0.00% (ϕ b)	15.26%
MG 2		15.47%		27.16%		15.29%
MG 3		17.65%		27.38%		16.52%
MG 4		14.57%		27.32%		14.90%
MG 5		13.78%		27.17%		14.83%
MG 6		18.84%		27.22%		15.54%
Average	0.00%; 0.00%	16.63%	26.82%; 16.97%	27.29%	0.00%; 0.00%	15.54%

Table I shows the results of different fault management methods for SPG faults. The following statements can be achieved for this case study:

1) DA-AFM performs similarly to centralized AFM in both indices, proving DA-AFM's accurate convergence.
2) DA-AFM outperforms the simple ride-through method in both indices, proving DA-AFM's superiority.

B. Double-phase-to-ground (DPG) fault

In this case study, a DPG fault occurs on phases a and b from 0.6s to 0.9s. The remaining voltages are 0.52 pu. The results of DA-AFM are shown in Fig. 7 (NMs' power, and phase a and phase b fault currents at fault locations) and Fig. 8 (NMs' voltages, currents, and DC voltages). As shown in Fig. 7, fault currents from the main grid and the total fault currents are controlled to be the same at 182.15 A for phase a and 212.92 A for phase b, making NMs' contributions to fault currents 0.00% for both faulty phases. Power ripples of

This article has been accepted for publication in a future issue of this journal, but has not been fully edited. Content may change prior to final publication. Citation information: DOI 10.1109/TPWRS.2020.2976044, IEEE Transactions on Power Systems

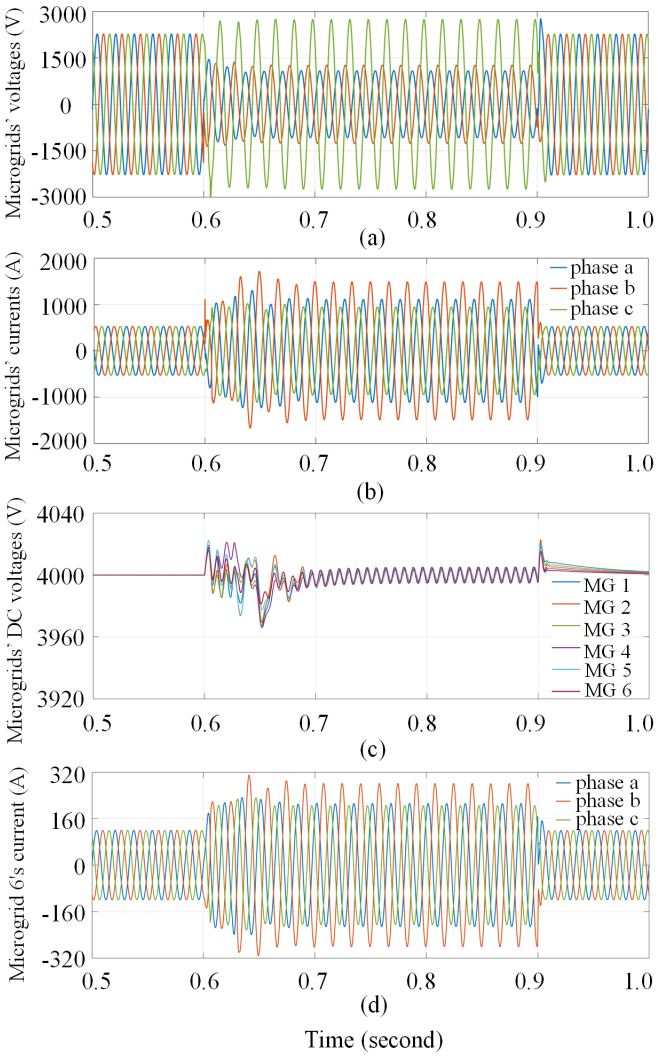

Fig. 8. DA-AFM for networked microgrids during double-phase-to-ground fault: (a) NMs' voltages at connection point; (b) NMs' currents to the main grid; (c) NMs' DC voltages; (d) microgrid 6's currents.

six microgrids are 19.48%, 15.47%, 17.65%, 14.57%, 13.78% and 18.84%, respectively, with an average value of 16.63%.

Fig. 9 shows the results with centralized AFM and the simple ride-through method for DPG fault. In centralized AFM (Fig. 9 (a) and (b)), the fault current contributions are 0.00% for both faulty phases, and six microgrids' power ripples are 16.90%, 15.29%, 16.52%, 14.90%, 14.83% and 14.78%, respectively, with an average value of 15.54%. In the simple ride-through method (Fig. 9 (c) and (d)), the fault current contributions are 26.82% (231.00/182.15) for phase a and 16.97% (249.05/212.92) for phase b, and the six microgrids' power ripples are 27.46%, 27.16%, 27.38%, 27.32%, 27.17% and 27.22%, respectively, with an average value of 27.29%.

Table II shows the results of different fault management methods for DPG faults. The following comparisons can be achieved for this case study:

1) DA-AFM performs similarly to centralized AFM in both indices, proving DA-AFM's accurate convergence.
2) DA-AFM outperforms the simple ride-through method, proving DA-AFM's superiority.

TABLE III
COMPARISON BETWEEN DIFFERENT FAULT MANAGEMENT METHODS FOR PHASE-TO-PHASE FAULT

	DA-AFM		A simple ride-through method		Centralized AFM	
	fault contribution	power ripples	fault contribution	power ripples	fault contribution	power ripples
MG 1	0.00%	6.66%	25.87%	37.39%	0.00%	7.93%
MG 2		6.34%		37.35%		7.04%
MG 3		6.33%		37.38%		7.83%
MG 4		4.87%		37.35%		6.90%
MG 5		4.70%		37.37%		6.49%
MG 6		4.98%		37.38%		6.44%
Average	0.00%	5.65%	25.87%	37.37%	0.00%	7.11%

C. Phase-to-phase fault

The simulated phase-to-phase fault occurs between phases a and b from 0.6s to 0.9s. The remaining phase-to-phase voltage is 0.52 pu. One difference between non-ground faults and ground faults is the expression for fault current contributions F_1. For phase-to-phase faults, F_1 is expressed as,

$$F_1 = \frac{1}{D}\left|\frac{[\mathrm{Re}(\mathbf{I}_a^M+\mathbf{I}_a^m)]^2+[\mathrm{Im}(\mathbf{I}_a^M+\mathbf{I}_a^m)]^2}{0.25[\mathrm{Re}(\mathbf{I}_a^M-\mathbf{I}_b^M)]^2+[\mathrm{Im}(\mathbf{I}_a^M-\mathbf{I}_b^M))]^2}-1\right| = \frac{1}{D}\left|\frac{[\mathrm{Re}(\mathbf{I}_b^M+\mathbf{I}_b^m)]^2+[\mathrm{Im}(\mathbf{I}_b^M+\mathbf{I}_b^m)]^2}{0.25[\mathrm{Re}(\mathbf{I}_a^M-\mathbf{I}_b^M)]^2+[\mathrm{Im}(\mathbf{I}_a^M-\mathbf{I}_b^M))]^2}-1\right| \quad (15)$$

where superscripts M, m denote variables related to the main grid and NMs, respectively. $\mathbf{I}_a^M+\mathbf{I}_a^m = -(\mathbf{I}_b^M+\mathbf{I}_b^m)$ is the fault current flowing throwing the fault resistor between phase a and phase b. The current $\frac{1}{2}(\mathbf{I}_a^M-\mathbf{I}_b^M)$ in the denominator has been largely used in relay setting for phase-to-phase faults [28], [29]. Minimizing fault current contributions for phase-to-phase faults means to make amplitudes of currents flowing through the fault as close as amplitudes of $\frac{1}{2}(\mathbf{I}_a^M-\mathbf{I}_b^M)$. When no microgrids are connected, the current flowing through the fault is exactly $\frac{1}{2}(\mathbf{I}_a^M-\mathbf{I}_b^M)$.

The results of DA-AFM, the simple ride-through method, and centralized AFM are shown in Table III. Voltage vectors and current vectors with DA-AFM are shown in Fig. 10. In DA-AFM, both the current flowing through the resistor ($\mathbf{I}_f$) and the current $\frac{1}{2}(\mathbf{I}_a^M-\mathbf{I}_b^M)$ have the same amplitude 201 A (Fig. 10 (c)), meaning fault current contributions are 0.00%. Power ripples of six microgrids are 6.66%, 6.34%, 6.33%, 4.87%, 4.70% and 4.98%, respectively, with an average value of 5.65%.

For centralized AFM, fault current contributions and average power ripples are 0.00% and 7.11%, respectively, both indices similar to DA-AFM. For the simple ride-through method, fault current contributions and average power ripples are 25.87% (201 A to 253 A) and 37.37%, respectively, both indices worse than DA-AFM. The following comparisons can be achieved for the case study of phase-to-phase faults:

1) DA-AFM performs similarly to centralized AFM in both indices, proving DA-AFM's accurate convergence.
2) DA-AFM outperforms the simple ride-through method, proving DA-AFM's superiority.

This article has been accepted for publication in a future issue of this journal, but has not been fully edited. Content may change prior to final publication. Citation information: DOI 10.1109/TPWRS.2020.2976044, IEEE Transactions on Power Systems

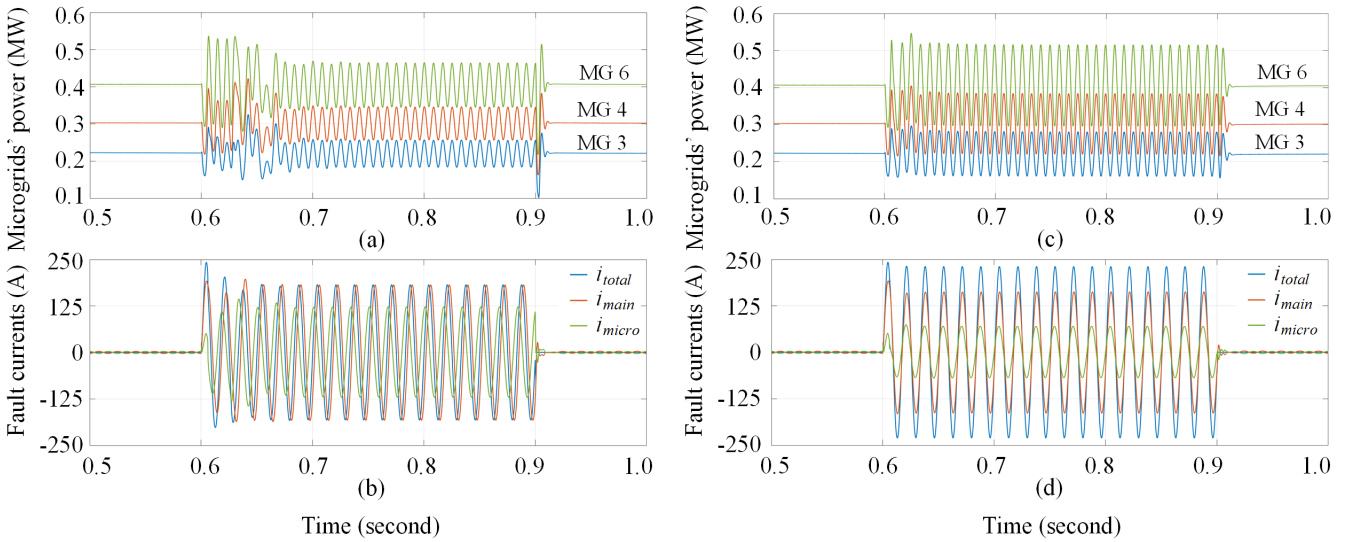

Fig. 9. Centralized AFM during double-phase-to-ground fault: (a) microgrids' output power and (b) phase a fault currents at fault locations. The simple ride-through method during double-phase-to-ground fault: (c) microgrids' output power and (d) phase a fault currents at fault locations.

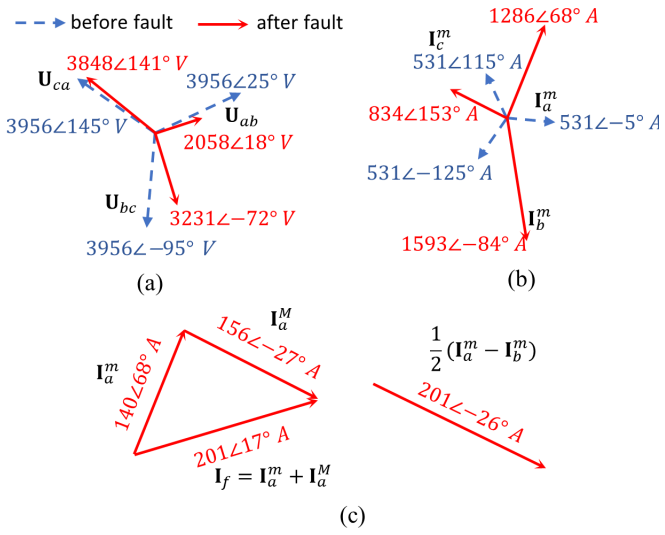

Fig. 10. Voltage vectors and current vectors with DA-AFM for phase-to-phase faults: (a) NMs phase-to-phase voltages, (b) NMs phase currents and (c) currents at fault locations, including phase a currents of NMs ($\mathbf{I}_a^m$), phase a current from the main grid ($\mathbf{I}_a^M$) and the current flowing through the fault ($\mathbf{I}_f$).

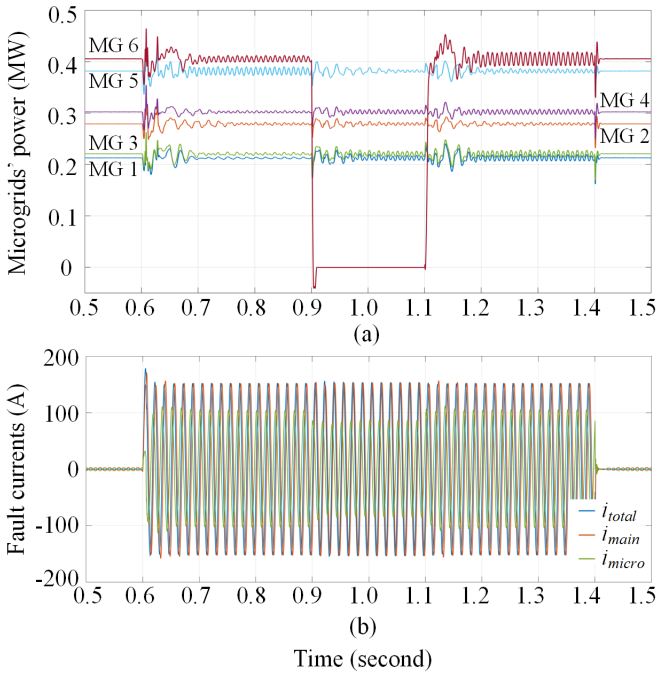

Fig. 11. Plug-and-play of DA-AFM during single-phase-to-ground fault: (a) six microgrids' output power to the main grid; (b) phase a currents at the fault location. Microgrid 6 is tripped off at 0.9s and connected back to the main grid at 1.1s.

D. Plug-and-Play of DA-AFM

In this section, the plug-and-play of DA-AFM is demonstrated. The single-phase-to-ground fault happens on phase a at 0.6s and is cleared at 1.4s, with a remaining voltage of 0.52 pu. Microgrid 6 disconnects from the main grid at 0.9s, and then connects back to the main grid at 1.1s.

Fig. 11 (a) and (b) shows the NM's power to the main grid and phase a fault currents at the fault location, respectively. After disconnection and connection, ripples of microgrid 1, microgrid 3 and microgrid 6 have increased, while ripples of microgrid 2, microgrid 4 and microgrid 5 have decreased. The average power ripples only have a negligible change, from 1.11% to 1.54%, and current contributions keep the same at 0%. The authors believe there are two main reasons for this little difference: 1. DA-AFM's computation is a distributed and asynchronous algorithm. Different runs result in different computation sequences for the six cores and therefore different intermediate states; 2. There may have been multiple local minima in a small area, and which minimum to reach is decided by initial operation points and computation sequence.

Overall, microgrids' power ripples and fault current contributions are kept at similarly low levels during disconnection and reconnection, demonstrating DA-AFM's excellent performance during plug-and-play.

This article has been accepted for publication in a future issue of this journal, but has not been fully edited. Content may change prior to final publication. Citation information: DOI 10.1109/TPWRS.2020.2976044, IEEE Transactions on Power Systems

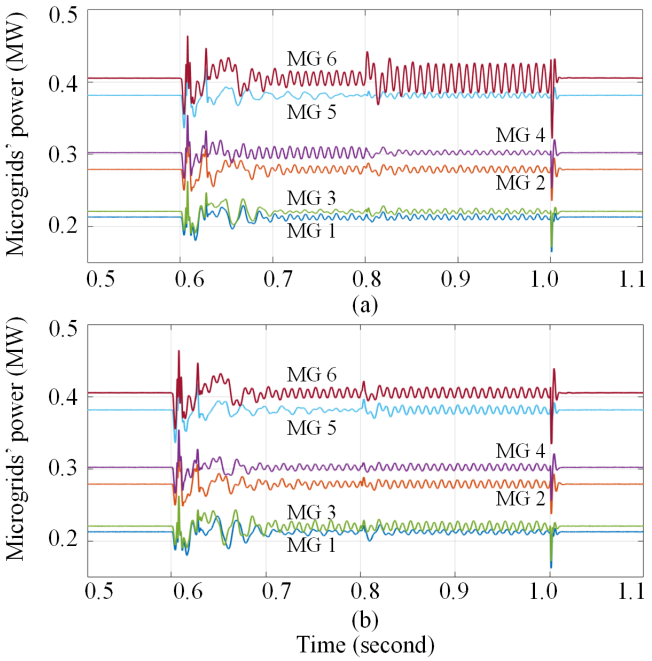

Fig. 12. DA-AFM's response to communication delay during single-phase-to-ground fault. Microgrids' output power to the main grid (a) without SDN and (b) with SDN. Delays happens at 0.8s. The fault lasts from 0.6s to 1.0s.

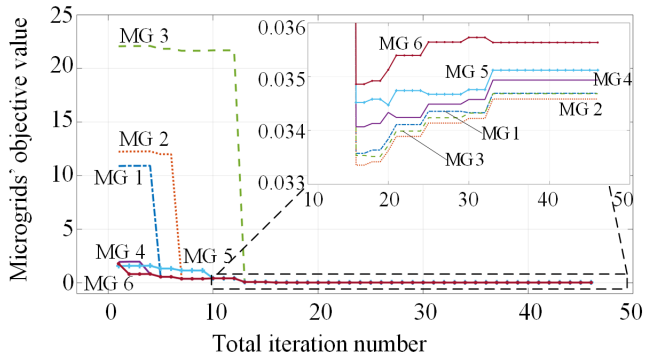

Fig. 13. Each microgrid's objective value at every iteration step.

TABLE IV
REAL-TIME PERFORMANCE OF DA-AFM BY ENDING OPTIMIZATION PREMATURELY

	DA-AFM with full iteration number		DA-AFM with 50% iteration number		DA-AFM with 30% iteration number	
	fault contributions	power ripples	fault contributions	power ripples	fault contributions	power ripples
SPG fault	0.00%	1.11%	0.00%	1.11%	0.00%	1.11%
DPG fault	0.00%; 0.00%	16.63%	0.00%; 0.00%	17.85%	0.00%; 0.00%	24.79%

E. Networking reconfiguration of SDN-enabled DA-AFM

This section evaluates SDN-enabled DA-AFM's resilience to communication delays. The single-phase-to-ground fault happens at 0.6s and is cleared at 1.0s. Phase a's remaining voltage is 0.52 pu. At 0.8s, there is 30 ms delay in a switch which microgrid 6's packets go through. SDN is able to detect the delay and then reroute microgrid 6's packet transfer to those available and undelayed links. Fig. 12 shows the NMs' power to the main grid without SDN and with SDN. Without SDN, the microgrids' overall power ripples increase after a delay happens. This occurs because the communication delay decreases certain microgrids' (microgrid 6 in our case) number of calculation iterations, leading to suboptimal results. With SDN, the ripples' magnitudes never deteriorate, which means SDN provides a performance guarantee for DA-AFM.

TABLE V
REAL-TIME PERFORMANCE OF DA-AFM BY MAKING OPTIMIZATION MODULES AND FEEDBACK CONTROL MODULES ASYNCHRONOUS

Lagging of optimization module (simulation steps)	Average power ripples		fault current contributions	
	SPG fault	DPG fault	SPG fault	DPG fault
0	1.11%	16.63%	0%	0%; 0%
10	1.17%	17.40%	0%	0%; 0%
20	1.39%	21.35%	0%	0%; 0%
30	1.56%	17.99%	0%	0%; 0%
40	1.51%	20.58%	0%	0%; 0%

F. Real-time performance of DA-AFM

In subsection III-B, two methods for the real-time realization of DA-AFM are mentioned: reducing iteration number by increasing the stop criteria, and making optimization modules and feedback control modules asynchronous. This subsection demonstrates these two methods' effectiveness.

Fig. 13 shows six microgrids' objective values at each iteration number for single-phase-to-ground fault. Even though the whole optimization process terminates after totally 46 iterations, NMs' objective values don't change too much after iteration number 18. Based on this property, DA-AFM's iterations can be reduced to increase its computation speed. Table IV shows the corresponding results. For single-phase-to-ground-fault, the performance with respect to fault contributions and power ripples remain the same even when the number of iterations is reduced to 30%. For double-phase-to-ground-fault, when the number of iterations is reduced to 30%, fault current contributions remain the same while average power ripples for NMs increase from 16.63% to 24.79%.

When optimization modules and feedback control modules are made asynchronous, feedback control modules use the newest available results from the optimization modules without waiting for their current computation. This is equivalent to introducing delays to optimization modules. Table V shows DA-AFM's performance by making optimization modules and feedback control modules asynchronous. The simulation step size is 50 μs. As delays increase, fault current contributions don't increase. This is because we assign a higher weight factor for fault current contributions in the formulation (7). As delays increase, average power ripples increase a little first and then fluctuate with small amplitudes. Optimization module delays do not dramatically affect DA-AFM performance because DA-AFM's formulation (7)-(13) use voltages and currents' amplitudes and angles instead of instant values.

This article has been accepted for publication in a future issue of this journal, but has not been fully edited. Content may change prior to final publication. Citation information: DOI 10.1109/TPWRS.2020.2976044, IEEE Transactions on Power Systems

TABLE VI
SCALABILITY OF DA-AFM

Number of microgrids	Objective value	Iterations per microgrid
6	0.0227	8.17
12	0.0323	10.50
18	0.0253	8.67
24	0.0258	10.67
30	0.0332	11.88
36	0.0312	7.90

TABLE VII
DA-AFM FOR SOLID FAULTS

Fault type	Fault contributions	Average power ripples
SPG fault	0.00%	1.89%
DPG fault	0.00%; 0.00%	98.56%
Phase-to-phase fault	0.00%	95.15%

After transients of about half a 60 Hz cycle ($\sim 0.008s$), amplitudes and angles of voltages and currents don't change much.

The real-time realization of DA-AFM is demonstrated with results in Table IV (by reducing iteration number) and Table V (by making feedback control modules and optimization modules asynchronous).

G. Scalability of DA-AFM

This subsection shows that DA-AFM can be scaled up for large numbers of microgrids. The numerical analyses in subsection IV-A to IV-F are conducted with six microgrids.

Fig. 14 shows each microgrid's objective value at every iteration step when the networked microgrids has 36 microgrids. As iteration increases, all the microgrids' objective values decrease until convergence.

Table VI shows the final objective value and iterations per microgrid when the NMs have a different number of microgrids. The results are achieved using the single-phase-to-ground fault case. As the numbers in the second column show, the final objective values of DA-AFM experience little change. This means that as the number of microgrids increases, DA-AFM can achieve the same level of performance with respect to fault current contributions and power ripples. The third column shows the average iteration number per microgrid will not increase as the number of microgrids increases. Given the results, the computation time should not increase.

Scalability of DA-AFM is demonstrated with results in Fig. 14 and Table. VI. The results show when the number of microgrids increases from 6 to 36, DA-AFM can keep performance at the same level without increasing computation time.

H. DA-AFM performance under miscellaneous situations

1) Results for solid ground faults. This part gives results of DA-AFM in case of solid faults, as shown in Table VII.

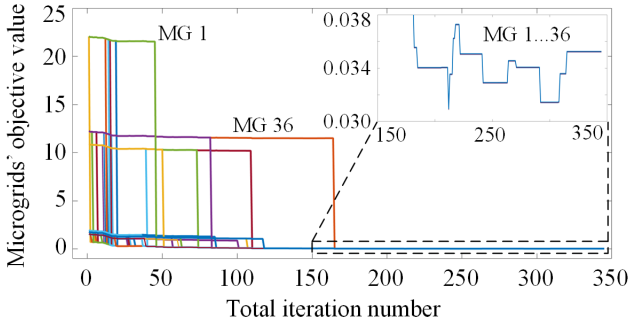

Fig. 14. Each microgrid's objective value at every iteration step when the networked microgrids has 36 microgrids. Objective values of 36 microgrids reach the same values as iteration increases.

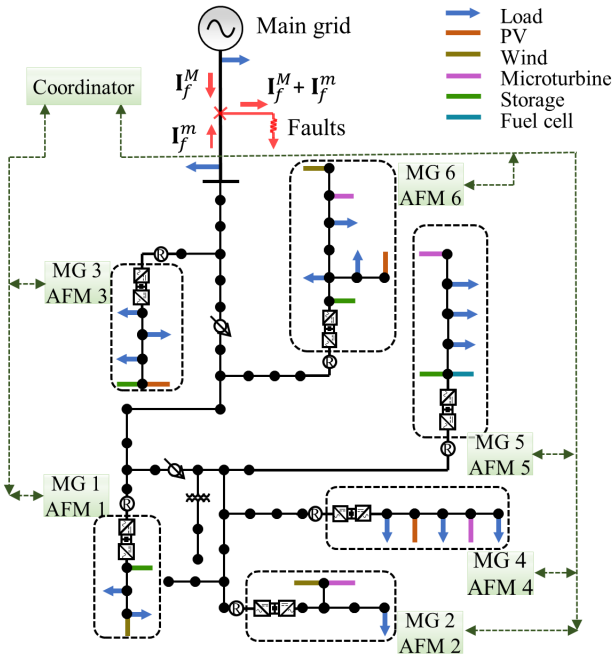

Fig. 15. DA-AFM for a networked microgrids system connected to a complex distribution network

During simulations, the ground resistors for ground faults and the fault resistors for phase-to-phase faults are set to 0 Ω.

According to Table VII, for single-phase ground faults, DA-AFM performs for solid faults as well as when voltage drops to 0.52 pu with respect to fault current contributions and power ripples. For double-phase ground faults and non-ground faults, the fault current contributions remain the same at 0.00% while power ripples have increased.

The reason for fault current contributions remaining the same at 0% for all three types of faults is that in formulation (7), fault current contributions F_1 have been given a higher weight factor. The reason for power ripples increasing for double-phase ground solid faults and non-ground solid faults is that asymmetry levels for these two types of faults have increased beyond systems' capacity. Power ripples for these two types of faults can be reduced by increasing current ratings, i.e., I_i^S in (10) and $I^{S,M}$ in (13).

2) Applicability to complex topology. To demonstrate DA-

AFM's performance under different network structures, six microgrids are connected to different points of a modified IEEE 34 feeder system, as shown in Fig. 15, instead of being connected at the same point of connection. The simulation results achieved with this 34 distribution feeder system are very similar to the simulation results achieved with topology shown in Fig.1. The results for single-phase-to-ground faults are shown in Fig. 4, Fig. 5 and Table I. The results for double-phase-to-ground faults are shown in Fig. 7, Fig. 8 and Table II.

The reason for getting the same results with this new topology is because this topology is radial and relatively small in size. This means at the fault location, the total currents from NMs is simply an addition of all microgrids' currents, which is also the case when all the microgrids are connected to the same point of connection. In the future, distribution systems with loops and of large size, or situations where microgrids are connected to different distribution systems will be considered. In these cases, relationships between a microgrid's output currents and the corresponding contribution currents at fault locations will be represented by matrices.

V. Conclusion

DA-AFM for NMs is designed to enable NMs' fault ride-through capabilities, facilitating the deep penetration of heterogeneous microgrids in the future. DA-AFM is formulated as an optimization problem, solved with the surrogate Lagrangian relaxation method, implemented with one CPU of multiple cores, and facilitated by software defined networking (SDN). DA-AFM's accurate convergence, excellence, plug-and-play, resilient to communication delay, real-time performance and scalability are demonstrated through case studies for NM systems of more than six microgrids. The method can be triggered immediately and overrides microgrids' primary control upon the detection of faults. The next step is to extend DA-AFM for managing both DC microgrids and hybrid microgrids and to integrate DER operations inside microgrids.

References

[1] P. Zhang and B. Wang, *Enabling Reliable Networked Microgrids for Distribution Grid Resiliency*, Grant Proposal for ECCS-1611095, National Science Foundation, 2016.

[2] P. Zhang, *Networked Microgrids*. Cambridge University Press, 2020.

[3] "IEEE standard for interconnection and interoperability of distributed energy resources with associated electric power systems interfaces," *IEEE Std 1547-2018*, pp. 1–138, April 2018.

[4] L. Ren, Y. Qin, Y. Li, P. Zhang, B. Wang, P. B. Luh, S. Han, T. Orekan, and T. Gong, "Enabling resilient distributed power sharing in networked microgrids through software defined networking," *Applied Energy*, vol. 210, pp. 1251 – 1265, 2018.

[5] M. Abdolkarimzadeh, M. Nazari-Heris, M. Abapour, and M. Sabahi, "A bridge-type fault current limiter for energy management of ac/dc microgrids," *IEEE Transactions on Power Electronics*, vol. 32, no. 12, pp. 9043–9050, 2017.

[6] T. Ghanbari and E. Farjah, "Unidirectional fault current limiter: An efficient interface between the microgrid and main network," *IEEE Transactions on Power Systems*, vol. 28, no. 2, pp. 1591–1598, May 2013.

[7] H. R. Baghaee, M. Mirsalim, and G. B. Gharehpetian, "Real-time verification of new controller to improve small/large-signal stability and fault ride-through capability of multi-der microgrids," *IET Generation, Transmission & Distribution*, vol. 10, no. 12, pp. 3068–3084, 2016.

[8] N. Rajaei, M. H. Ahmed, M. M. Salama, and R. K. Varma, "Fault current management using inverter-based distributed generators in smart grids," *IEEE Transactions on Smart Grid*, vol. 5, no. 5, pp. 2183–2193, 2014.

[9] A. Junyent-Ferre, O. Gomis-Bellmunt, T. C. Green, and D. E. Soto-Sanchez, "Current control reference calculation issues for the operation of renewable source grid interface vscs under unbalanced voltage sags," *IEEE Transactions on Power Electronics*, vol. 26, no. 12, pp. 3744–3753, Dec 2011.

[10] Y. Zhang and C. Qu, "Direct power control of a pulse width modulation rectifier using space vector modulation under unbalanced grid voltages," *IEEE Transactions on Power Electronics*, vol. 30, no. 10, pp. 5892–5901, Oct 2015.

[11] W. Wan, Y. Li, B. Yan, M. A. Bragin, J. Philhower, P. Zhang, P. B. Luh, and G. Warner, "Active fault management for microgrids," in *44th Annual Conference of the IEEE Industrial Electronics Society (IECON)*, October 2018, pp. 1–6.

[12] W. Wan, Y. Li, B. Yan, M. A. Bragin, J. Philhower, P. Zhang, and P. B. Luh, "Active fault management for networked microgrids," in *2019 IEEE Power and Energy Society General Meeting (PESGM)*, August 2019, pp. 1–5, to be published.

[13] J. M. Guerrero, J. C. Vasquez, J. Matas, L. G. de Vicuna, and M. Castilla, "Hierarchical control of droop-controlled ac and dc microgrids—a general approach toward standardization," *IEEE Transactions on Industrial Electronics*, vol. 58, no. 1, pp. 158–172, Jan 2011.

[14] A. L. Dimeas and N. D. Hatziargyriou, "Operation of a multiagent system for microgrid control," *IEEE Transactions on Power Systems*, vol. 20, no. 3, pp. 1447–1455, Aug 2005.

[15] M. A. Bragin and P. B. Luh, "Distributed and asynchronous unit commitment and economic dispatch," in *2017 IEEE Power Energy Society General Meeting*, July 2017, pp. 1–5.

[16] Z. Zhang and M. Chow, "Convergence analysis of the incremental cost consensus algorithm under different communication network topologies in a smart grid," *IEEE Transactions on Power Systems*, vol. 27, no. 4, pp. 1761–1768, Nov 2012.

[17] Z. Wang, B. Chen, J. Wang, M. M. Begovic, and C. Chen, "Coordinated energy management of networked microgrids in distribution systems," *IEEE Transactions on Smart Grid*, vol. 6, no. 1, pp. 45–53, Jan 2015.

[18] P. Goransson, C. Black, and T. Culver, *Software defined networks: a comprehensive approach*. Morgan Kaufmann, 2016.

[19] D. E. Comer, *Internetworking with TCP/IP: Principles, Protocols, and Architecture*. Prentice Hall, 2013, vol. 1.

[20] D. Kreutz, F. M. Ramos, P. Verissimo, C. E. Rothenberg, S. Azodolmolky, and S. Uhlig, "Software-defined networking: A comprehensive survey," *Proceedings of the IEEE*, vol. 103, no. 1, pp. 14–76, 2015.

[21] M. Di Somma, B. Yan, N. Bianco, G. Graditi, P. B. Luh, L. Mongibello, and V. Naso, "Operation optimization of a distributed energy system considering energy costs and exergy efficiency," *Energy Conversion and Management*, vol. 103, pp. 739–751, 2015.

[22] M. A. Bragin, P. B. Luh, and B. Yan, "Asynchronous coordination of distributed mixed-integer linear subsystems via surrogate lagrangian relaxation," under review.

[23] X. Zhao, P. B. Luh, and J. Wang, "Surrogate gradient algorithm for lagrangian relaxation," *Journal of optimization Theory and Applications*, vol. 100, no. 3, pp. 699–712, 1999.

[24] M. A. Bragin, P. B. Luh, J. H. Yan, N. Yu, and G. A. Stern, "Convergence of the surrogate lagrangian relaxation method," *Journal of Optimization Theory and applications*, vol. 164, no. 1, pp. 173–201, 2015.

[25] P. Piya, M. Ebrahimi, M. Karimi-Ghartemani, and S. A. Khajehoddin, "Fault ride-through capability of voltage-controlled inverters," *IEEE Transactions on Industrial Electronics*, vol. 65, no. 10, pp. 7933–7943, Oct 2018.

[26] F. Zheng, Y. Chen, Y. Zhang, Y. Lın, and M. Guo, "Low voltage ride-through capability improvement of microgrid using a hybrid coordination control strategy," *Journal of Renewable and Sustainable Energy*, vol. 11, no. 3, p. 034102, 2019.

[27] Jayakrishnan R and Sruthy V, "Fault ride through augmentation of microgrid," in *2015 International Conference on Technological Advancements in Power and Energy (TAP Energy)*, June 2015, pp. 357–362.

[28] A. A. Girgis, C. M. Fallon, and D. L. Lubkeman, "A fault location technique for rural distribution feeders," *IEEE Transactions on Industry Applications*, vol. 29, no. 6, pp. 1170–1175, Nov 1993.

[29] Zhang Qingchao, Zhang Yao, Song Wennan, Yu Yixin, and Wang Zhigang, "Fault location of two-parallel transmission line for nonearth fault using one-terminal data," *IEEE Transactions on Power Delivery*, vol. 14, no. 3, pp. 863–867, July 1999.

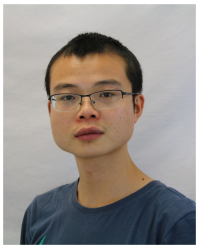

Wenfeng Wan (S'17) received the B.S. and M.S. degrees in electrical engineering from Xi'an Jiaotong University, Xi'an, China, in 2010 and 2013, respectively. He was with City University of Hong Kong, Hong Kong, from 2013 to 2017, first as a research assistant and then a graduate student. He is currently working toward the Ph.D. degree in electrical engineering with Stony Brook University, NY, USA. His current research focus is control and dynamics for renewable energy, microgrids, and power systems.

Mikhail A. Bragin (S'11−M'17) received the B.S. and M.S. degrees in mathematics from Voronezh State University, Voronezh, Russia, in 2004, the M.S. degree in physics and astronomy from the University of Nebraska-Lincoln, Lincoln, NE, USA, in 2006, and the M.S. and Ph.D. degrees in electrical and computer engineering from the University of Connecticut, Storrs, CT, USA, in 2014 and 2016, respectively. He is currently an Assistant Research Professor in electrical and computer engineering with the University of Connecticut. His research interests include mathematical optimization, including power system optimization, grid integration of renewables (wind and solar), energy-based operation optimization of distributed energy systems, and scheduling of manufacturing systems.

Bing Yan (S'11−M'17) received the B.S. degree from the Renmin University of China, Beijing, China, in 2010, and the M.S. and Ph.D. degrees from the University of Connecticut, Storrs, CT, USA, in 2012 and 2016, respectively. She is currently an Assistant Professor with the Department of Electrical and Microelectronic Engineering, Rochester Institute of Technology (RIT), Rochester, NY, USA. Before joining RIT, she was an assistant research professor in the Department of Electrical and Computer Engineering, University of Connecticut. Her research interests include power system operation optimization, grid integration of renewables, operation optimization of microgrids and distributed energy systems, scheduling of manufacturing systems, and mixed-integer linear optimization.

Yanyuan Qin (S'16) received the B.S. degree in automation from the Nanjing University of Aeronautics and Astronautics, China, in 2011, and the M.S. degree in control science and engineering from Shanghai Jiao Tong University, China, in 2014. He is currently pursuing the Ph.D. degree with the Computer Science and Engineering Department, University of Connecticut. His research interests are in software-defined networking and wireless networks.

Jason Philhower (M'07−SM'13) received the B.S. and M.E. degrees in electrical engineering from University of Hartford, West Hartford, CT, USA in 2008 and Worcester Polytechnic, Worcester MA, USA, in 2016, respectively. He is currently working toward the Ph.D. degree in electrical engineering at the University of Connecticut, Storrs, CT, USA. He is the current vice chair and former chair of the IEEE Power Energy Society, Connecticut Chapter. He is a Senior Electrical Engineer at POWER Engineers, Inc and a registered professional engineer in ten (10) states. His research interests are power systems and microgrids system stability.

Peng Zhang (M'07−SM'10) received the Ph.D.degree in Electrical Engineering from the University of British Columbia, Vancouver, BC, Canada, in 2009. He is a SUNY Empire Innovation Professor at Stony Brook University, NY, USA. He was a Francis L. Castleman Associate Professor and a Centennial Associate Professor at the University of Connecticut, Storrs, CT, USA, from 2017 to 2019. He was a System Planning Engineer at BC Hydro and Power Authority, Vancouver, during 2006-2010. His research interests include networked microgrids, programmable microgrids, cyber resilience, formal methods and reachability analysis, and quantum engineering.
Dr. Zhang is an individual member of CIGRÉ. He is an Editor for the IEEE Transactions on Power Systems, the IEEE Transactions on Sustainable Energy and the IEEE Power and Energy Society Letters, an Associate Editor for the IEEE Journal of Oceanic Engineering and the IEEE Transactions on Industrial Electronics.

Peter B. Luh (S'77–M'80–SM'91–F'95–LF'16) received the B.S. degree from the National Taiwan University, Taipei, Taiwan, the M.S. degree from the Massachusetts Institute of Technology, Cambridge, MA, USA, and the Ph.D. degree from Harvard University, Cambridge, MA, USA. Since 1980, he has been with the University of Connecticut, Storrs, CT, USA, and is currently a Board of Trustees Distinguished Professor and the SNET Professor of Communications and Information Technologies. His research interests include smart grid, intelligent manufacturing, and energy smart buildings. He was the founding Editor-in-Chief of IEEE Transactions on Automation Science and Engineering, the Chair of IEEE TAB Periodicals Committee for the 2018-19 term, and the Chair of IEEE TAB Periodicals Review and Advisory Committee for the 2020-21 term.